Axisymmetric multiphase lattice Boltzmann method

Axisymmetric multiphase lattice Boltzmann method

Sudhir Srivastava,[1] Prasad Perlekar,[1,2] Jan H. M. ten Thije Boonkkamp,[3] Nishith Verma,[4] and Federico Toschi[1,5]

[1]*Department of Applied Physics, Department of Mathematics and Computer Science and J.M. Burgerscentrum, Eindhoven University of Technology, P.O. Box 513, 5600 MB Eindhoven, The Netherlands*

[2]*Centre for Interdisciplinary Sciences, TIFR, 21 Brundavan Colony, Narsingi, Hyderabad 500075, India*

[3]*Department of Mathematics and Computer Science and J.M. Burgerscentrum, Eindhoven University of Technology, P.O. Box 513, 5600 MB Eindhoven, The Netherlands*

[4]*Department of Chemical Engineering, Indian Institute of Technology Kanpur, Kanpur 208016, India*

[5]*IAC, CNR, Via dei Taurini 19, I-00185 Roma, Italy*

(Received 26 February 2013; published 25 July 2013)

A lattice Boltzmann method for axisymmetric multiphase flows is presented and validated. The method is capable of accurately modeling flows with variable density. We develop the classic Shan-Chen multiphase model [Phys. Rev. E **47**, 1815 (1993)] for axisymmetric flows. The model can be used to efficiently simulate single and multiphase flows. The convergence to the axisymmetric Navier-Stokes equations is demonstrated analytically by means of a Chapmann-Enskog expansion and numerically through several test cases. In particular, the model is benchmarked for its accuracy in reproducing the dynamics of the oscillations of an axially symmetric droplet and on the capillary breakup of a viscous liquid thread. Very good quantitative agreement between the numerical solutions and the analytical results is observed.

DOI: 10.1103/PhysRevE.88.013309 PACS number(s): 47.11.−j, 05.20.Dd, 47.55.df, 47.61.Jd

I. INTRODUCTION

Multiphase flows occur in a large variety of phenomena, in nature and industrial applications alike. In both types of applications it is often necessary to accurately and efficiently simulate the dynamics of interfaces under different flow conditions. A paradigmatic industrial application concerns the formation of small ink droplets from inkjet printer nozzles [1]. When both flow geometry and initial conditions display axial symmetry, one expects that the flow will preserve that symmetry at any later time. Under such conditions it is advantageous to employ numerical methods capable of exploiting the symmetry of the problem. The computational costs of a three-dimensional (3D) axisymmetric simulation is very close to that of two dimensions, presenting thus a considerable advantage over fully 3D simulations. When one deals with multiphase methods characterized by diffused interfaces, such as the ones common in the lattice Boltzmann method, the availability of additional computational resources allows one to decrease the interface width with respect to the other characteristic length scales in the problem. The possibility to get closer to the "sharp-interface" limit has thus a direct impact on the accuracy of the numerical solutions for diffuse interface multiphase solvers.

The lattice Boltzmann method (LBM) [2] has been widely employed to study multiphase flows in complex geometries under both laminar and turbulent flow conditions [3]. In recent years several implementations of the axisymmetric LBM for single-phase systems have been proposed [4–9], while, in comparison, relatively little attention has been devoted to the case of the multiphase flow [10,11].

The aim of the present paper is to introduce an accurate and efficient algorithm to study generic axisymmetric, density-varying flows and in particular multiphase flows. The proposed algorithm is easy to implement, is accurate, and its multiphase model builds upon the widely used Shan-Chen model [12,13]. One particular advantage of having the axisymmetric implementation of the Shan-Chen model is that it allows one to retain the same parameters of the fully 3D model (e.g., coupling strength, surface tension, and phase diagram) thus allowing us to easily switch between axisymmetric and full 3D Shan-Chen investigations, according to what is needed.

The paper is organized as follows. In Sec. II we present our lattice Boltzmann method. In Secs. III and IV we present the results of several benchmarks of the method against single and multiphase flows, respectively. In Sec. V conclusions are drawn. The derivation of the additional terms for the axisymmetric LBM model is presented in the Appendix.

II. MODEL

A. Multiphase lattice Boltzmann method

In this section we introduce the notation and quickly recall the basics of the Shan-Chen LBM; in particular we focus on the 2D and nine velocities (D2Q9) Shan-Chen (SC) model for multiphase flow [12,13]. The LBM is defined on a Cartesian, 2D lattice together with the nine velocities $\mathbf{c}_i$ and distribution functions f_i. The time evolution of the populations is a combination of free streaming and collisions:

$$f_i(\mathbf{x}+\mathbf{c}_i\delta t, t+\delta t) = f_i(\mathbf{x},t) - \frac{1}{\tau}\left[f_i(\mathbf{x},t) - f_i^{\mathrm{eq}}(\rho,\mathbf{u}^{\mathrm{eq}})\right]. \tag{1}$$

In the particular case of Eq. (1), we have further made use of the so-called BGK approximation where a single relaxation time τ is used to relax the population distributions towards the equilibrium distributions f_i^{eq}. In our notations the relaxation parameter τ is scaled by the time step δt. The kinematic viscosity of the fluid ν is related to the relaxation parameter τ by $\nu = c_s^2\delta t\,(\tau - 0.5)$, where $c_s = \sqrt{1/3}$ is the speed of sound for the D2Q9 model. The fluid density is defined as $\rho = \sum_i f_i$. In the SC model the internal or external force $\mathbf{F}$ is added to

the system by shifting the equilibrium velocity as [12,13]

$$\mathbf{u}^{\mathrm{eq}} = \frac{1}{\rho}\left(\sum_i \boldsymbol{c}_i f_i + \tau\, \delta t\, \mathbf{F}\right), \tag{2}$$

while the hydrodynamic velocity is defined as

$$\mathbf{u} = \frac{1}{\rho}\left(\sum_i \boldsymbol{c}_i f_i + \frac{\delta t}{2}\mathbf{F}\right). \tag{3}$$

The short-range (first neighbors) Shan-Chen force $\mathbf{F}(\mathbf{x})$ at position $\mathbf{x}$ is defined as

$$\mathbf{F}(\mathbf{x}) = -G\psi(\mathbf{x})\sum_i W_i \psi(\mathbf{x}+\mathbf{c}_i\delta t)\mathbf{c}_i, \tag{4}$$

where G is the interaction strength, and the W_i's are the lattice dependent weights. The density functional is $\psi(\rho(\mathbf{x})) = \rho_0[1-\exp(-\rho(\mathbf{x})/\rho_0)]$ where ρ_0 is a reference density and is equal to unity for the results presented in this paper. From this setting it follows that the bulk pressure p_{NI} and pressure tensor $P_{\alpha\beta}$ (for $\delta t = 1$) are given by

$$p_{\mathrm{NI}} = c_s^2\rho + \frac{c_s^2 G}{2}\psi(\rho)^2, \tag{5}$$

$$P_{\alpha\beta} = \left(c_s^2\rho + \frac{c_s^2 G}{2}\psi^2 + \frac{c_s^4 G}{2}\psi\nabla_{\mathbf{c}}^2\psi + \frac{c_s^4 G}{4}|\,\nabla_{\mathbf{c}}\,\psi|^2\right)\delta_{\alpha\beta} - \frac{c_s^4 G}{2}\partial_\alpha\psi\,\partial_\beta\psi + \left(\tau-\frac{1}{2}\right)^2\frac{1}{\rho}F_\alpha F_\beta, \tag{6}$$

respectively, and the surface tension γ_{lv} is given by

$$\gamma_{\mathrm{lv}} = -\frac{G c_s^4}{2}\int_{-\infty}^{\infty}(\nabla_{\mathbf{c}}\psi\cdot\hat{\mathbf{n}})^2\, dn, \tag{7}$$

where $\delta_{\alpha\beta}$ is the Kronecker δ function, $\hat{\mathbf{n}}$ is the unit vector normal to the interface, and $\nabla_{\mathbf{c}}$ and $\nabla_{\mathbf{c}}^2$ are the 2D Cartesian gradient and Laplacian operator, respectively (see [13–15] for details). Varying the interaction strength G and choosing an average density, it can be shown that the system can phase separate and model the coexistence of a liquid and its vapor. This multiphase system is characterized by a larger density in the liquid phase and a lower density in the vapor phase and by a surface tension at the interface separating the two phases. For the scheme proposed in Refs. [12,13] the surface tension given by Eq. (7) should have a τ-correction term, which is due to the last term of Eq. (6), and hence the surface tension is given by

$$\tilde{\gamma}_{\mathrm{lv}} = -\frac{G c_s^4}{2}\int_{-\infty}^{\infty}(\nabla_{\mathbf{c}}\psi\cdot\hat{\mathbf{n}})^2\, dn + \left(\tau-\frac{1}{2}\right)^2\int_{-\infty}^{\infty}(\mathbf{F}\cdot\hat{\mathbf{n}})^2\frac{1}{\rho}\, dn. \tag{8}$$

The τ-correction term in Eq. (8) is the consequence of the choice of the scheme used for adding the external or internal forces in LBE, for example, if we use the force incorporation scheme proposed in Ref. [16] the surface tension should not have the τ correction.

B. Axisymmetric Navier-Stokes equations

When the boundary conditions, the initial configuration, and all external forces are axisymmetric, one does expect that the solution of the Navier-Stokes (NS) equations will preserve the axial symmetry at any later time. The continuity and NS equations in the cylindrical coordinates (z,r,θ), in absence of external forces read

$$\partial_t\rho + \partial_\beta(\rho u_\beta) = -r^{-1}\rho u_r, \tag{9}$$

and

$$\rho(\partial_t u_z + u_\beta\partial_\beta u_z) = -\partial_z p + \partial_\beta[\mu(\partial_\beta u_z + \partial_z u_\beta)] + r^{-1}\mu(\partial_r u_z + \partial_z u_r), \tag{10a}$$

$$\rho(\partial_t u_r + u_\beta\partial_\beta u_r) = -\partial_r p + \partial_\beta[\mu(\partial_\beta u_r + \partial_r u_\beta)] + 2\mu\partial_r(r^{-1}u_r), \tag{10b}$$

respectively, where $\mu = \nu\rho$, is the dynamic viscosity and ν is the kinematic viscosity of the fluid. The index β runs over the set $\{z,r\}$, and when an index appears twice in a single term it represents the standard Einstein summation convention. In principle an axisymmetric flow may have an azimuthal component of the velocity field, u_θ. In Eqs. (9) and (10) we assume that the flows that we consider have no swirl, i.e., $u_\theta = 0$, and that other hydrodynamic variables are independent of θ. We can thus write $u_r = u_r(z,r;t)$, $u_\theta = 0$, $u_z = u_z(z,r;t)$, and $\rho = \rho(z,r;t)$.

The axisymmetric version of the continuity and NS equations have been recast in a form, Eqs. (9) and (10), to easily highlight the similarities with respect to 2D flows in a (z,r) plane. Our approach employs a 2D LBM to solve for the two-dimensional part of the equations and explicitly treat the additional terms.

The continuity equation differs from the purely 2D one because of the presence of a source or sink term on the right hand side of Eq. (9); this term is responsible for a locally increasing mass whenever fluid is moving towards the axis, and for decreasing mass when moving away. The physical role of this term is to maintain 3D mass conservation (a density ρ at a distance r must be weighted with a $2\pi r$ factor).

The NS equations have also been rewritten in a way to highlight the 2D equations. The additional contributions that make the 3D axisymmetric equations differ from the 2D ones are the terms $r^{-1}\mu(\partial_r u_z + \partial_z u_r)$ and $2\mu\partial_r(r^{-1}u_r)$ on the right hand side of Eqs. (10). In our LBM model these terms are also explicitly evaluated and added as additional forcing terms.

The idea to model the 3D axisymmetric LBM with a 2D LBM supplemented with appropriate source terms has already been employed in a number of studies, for single-phase axisymmetric LBM models [4,5,17,18] and for the multiphase LBM as well [10,11]. Here we will develop an axisymmetric version of the Shan-Chen model [12,13].

From here onwards we will use the following notations: $\mathbf{x} = (z,r)$, $\mathbf{u} = (u_z,u_r)$, and $\nabla_{\mathbf{c}} = (\partial_z,\partial_r)$, where the z axis is the horizontal axis and the r axis is the vertical axis.

C. LBM for axisymmetric flow

The first step in deriving a LBM for axisymmetric multiphase flows is to derive a model that can properly deal with density variations. In particular, the LBM should recover the axisymmetric continuity Eq. (9) and NS Eqs. (10) by means of a Chapman-Enskog (CE) expansion in the long-wavelength

and long-time-scale limit. In order to derive such a model we start from the 2D LBM with the addition of appropriate space- and time-varying microscopic sources h_i (see also [4,5,17,18]). We employ the following lattice Boltzmann equation:

$$f_i(\mathbf{x}+\mathbf{c}_i\delta t,t+\delta t)-f_i(\mathbf{x},t) = -\frac{1}{\tau}\left[f_i(\mathbf{x},t)-f_i^{\mathrm{eq}}(\rho,\mathbf{u}^{\mathrm{eq}})\right]+\delta t h_i(\mathbf{x}+\mathbf{c}_i\delta t/2,t+\delta t/2), \tag{11}$$

where the source terms h_i, are evaluated at fractional time steps. It can be shown, see the Appendix, that when the additional term h_i in Eq. (11) has the following form:

$$h_i = W_i\left(-\frac{\rho u_r}{r}+\frac{1}{c_s^2}(c_{iz}H_z+c_{ir}H_r)\right), \tag{12}$$

with

$$H_z = \frac{c_{iz}}{r}(\mu(\partial_r u_z+\partial_z u_r)-\rho u_r u_z), \tag{13a}$$

$$H_r = \frac{c_{ir}}{r}\left[2\mu\left(\partial_r u_r-\frac{u_r}{r}\right)-\rho u_r^2\right], \tag{13b}$$

the CE expansion of Eq. (11) provides the axisymmetric version of the continuity and of the NS Eqs. (9) and (10), respectively. Details on the CE expansion are reported in the Appendix. The equations introduced here are enough to describe a fluid with variable density in axisymmetric geometry. We performed validations of the numerical model (not reported) by observing the behavior of the volume for the case of a droplet approaching the axis. While the 2D volume in the system was not conserved, the properly defined 3D volume was conserved with good accuracy.

D. LBM for axisymmetric multiphase flow

With a lattice Boltzmann method capable of handling density variations the additional steps towards the definition of the axisymmetric version of the SC multiphase model only consists in the correct definition of the SC force. The expression for the SC force in three dimensions is

$$\mathbf{F}(\mathbf{x}) = -G\psi(\mathbf{x})\sum_i W_i\psi(\mathbf{x}+\mathbf{c}_i\delta t)\mathbf{c}_i. \tag{14}$$

To find the lattice expression for the axisymmetric case we proceed by passing to the continuum limit, by expressing the continuum force in cylindrical coordinates and then by separating the 2D SC force from the additional axisymmetric contributions.

By means of a Taylor expansion for $\psi(\mathbf{x}+\mathbf{c}_i\delta t)$ one easily obtains the following continuum expression for the SC force [15]:

$$\mathbf{F}(\mathbf{x}) = -Gc_s^2\,\delta t\,\psi(\mathbf{x})\nabla\psi(\mathbf{x})-\frac{G}{2}c_s^4(\delta t)^3\psi(\mathbf{x})\nabla(\nabla^2\psi(\mathbf{x})) + O[(\delta t)^5]. \tag{15}$$

The above force expression is lattice independent and holds true for any 3D coordinate system. We restrict Eq. (15) to the case of axisymmetric flows by expressing both the gradient ∇ and the Laplace ∇^2 operators in cylindrical coordinates given by $\nabla\equiv(\partial_z,\partial_r)=\nabla_{\mathbf{c}}$ and $\nabla^2\equiv(\partial_{zz}+\partial_{rr}+r^{-1}\partial_r)=\nabla_{\mathbf{c}}^2+r^{-1}\partial_r$. Thus, in the axisymmetric case, Eq. (15) reduces to

$$\mathbf{F}(\mathbf{x}) = -Gc_s^2\,\delta t\,\psi(\mathbf{x})\nabla_{\mathbf{c}}\psi(\mathbf{x})-\frac{G}{2}c_s^4(\delta t)^3\psi(\mathbf{x})\nabla_{\mathbf{c}}\left(\nabla_{\mathbf{c}}^2\psi(\mathbf{x})\right) + \mathbf{F}^{\gamma,\mathrm{sym}}(\mathbf{x})+O[(\delta t)^5], \tag{16}$$

where

$$\mathbf{F}^{\gamma,\mathrm{sym}}(\mathbf{x}) = -\frac{G}{2}c_s^4(\delta t)^3\psi(\mathbf{x})\nabla_{\mathbf{c}}(r^{-1}\partial_r\psi(\mathbf{x})). \tag{17}$$

From Eq. (16) we immediately recognize that the first two terms on the right hand side are the ones that one obtains from the Shan-Chen model in two dimensions. The last term in Eq. (16), $\mathbf{F}^{\gamma,\mathrm{sym}}$, is the additional term responsible for the three dimensionality. This extra contributions needs to be accurately taken into account in order to model the axisymmetric Shan-Chen multiphase systems in three dimensions. In particular, this term is extremely important in order to correctly implement a 3D surface tension force which responds to curvatures, both along the axis and in the azimuthal direction. The two components of the additional term can be rewritten as

$$F_z^{\gamma,\mathrm{sym}} = -\frac{G}{2}c_s^4(\delta t)^3\psi r^{-1}\partial_{zr}\psi, \tag{18a}$$

$$F_r^{\gamma,\mathrm{sym}} = -\frac{G}{2}c_s^4\psi(\delta t)^3(r^{-1}\partial_{rr}\psi-r^{-2}\partial_r\psi). \tag{18b}$$

The evaluation of the terms $F_z^{\gamma,\mathrm{sym}}$ and $F_r^{\gamma,\mathrm{sym}}$ requires an approximation for the derivatives accurate up to order $(\delta t)^4$ or higher. Such an accuracy ensures the isotropy of the "reconstructed" 3D axisymmetric Shan-Chen force and thus the isotropy of the resulting surface tension along the interface.

In our implementation we used the following isotropic fifth-order accurate finite difference approximations on the D2Q9 lattice (see Fig. 1). For a scalar valued function $\phi(\mathbf{x})$ it reads

$$\partial_r\phi(\mathbf{x}) = \frac{1}{36}\sum_{i=1}^{8}[8\phi(\mathbf{x}+\mathbf{c}_i\delta t)-\phi(\mathbf{x}+2\mathbf{c}_i\delta t)]c_{ir} + O[(\delta t)^5], \tag{19a}$$

$$\partial_{rr}\phi(\mathbf{x}) = \frac{1}{36}\sum_{i=1}^{8}[8\partial_r\phi(\mathbf{x}+\mathbf{c}_i\delta t)-\partial_r\phi(\mathbf{x}+2\mathbf{c}_i\delta t)]c_{ir} + O[(\delta t)^5], \tag{19b}$$

$$\partial_{zr}\phi(\mathbf{x}) = \frac{1}{12}[-\partial_r\phi(\mathbf{x}+2\mathbf{c}_1\delta t)+8\partial_r\phi(\mathbf{x}+\mathbf{c}_1\delta t) - 8\partial_r\phi(\mathbf{x}+\mathbf{c}_3\delta t)+\partial_r\phi(\mathbf{x}+2\mathbf{c}_3\delta t)]+O[(\delta t)^6], \tag{19c}$$

where $\partial_r\phi(\mathbf{x})$ in Eq. (19c) is approximated as

$$\partial_r\phi(\mathbf{x}) = \tfrac{1}{12}[-\phi(\mathbf{x}+2\mathbf{c}_2\delta t)+8\phi(\mathbf{x}+\mathbf{c}_2\delta t) - 8\phi(\mathbf{x}+\mathbf{c}_4\delta t)+\phi(\mathbf{x}+2\mathbf{c}_4\delta t)]+O[(\delta t)^6]. \tag{19d}$$

From the SC model the present axisymmtric implementation does inherit all advantages as well as the limitations. One of the limitations is the relatively small density contrast

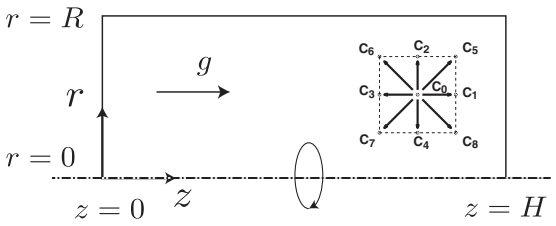

FIG. 1. Schematics of the axisymmetric geometry, eventually in presence of gravity or an external force aligned with the z axis. Schematics also show the lattice velocities for the D2Q9 model.

that can be achieved. Other multiphase LBM models, for which a similar axisymmetric extension could similarly be worked out, may allow us to achieve larger density contrasts. In the SC model both the density ratio ρ_l/ρ_v and the surface tension γ depend upon a single parameter G. Decreasing the value of G increases both the surface tension and the density ratio between two phases. Higher surface tension gives smaller interface width that leads to higher truncation error in the gradient approximation at the interface. This makes the numerical scheme unstable for too high values of G. As a rule of thumb, a density ratio of $\rho_l/\rho_v \leqslant 35$ ($G \geqslant -6.0$) still ensures the stability of the SC model. Therefore, the current axisymmetric SC model, as much as the standard SC model, is limited to a density ratio around 35.

E. Boundary conditions

In axisymmetric flows the boundary conditions for the distribution functions f_i need to be prescribed at all boundaries including the axis. In our approach we impose boundary conditions before the streaming step (prestreaming). We use midgrid point specular reflection boundary conditions on the axis [19]; this choice allows us to avoid the singularity due to the force terms containing $1/r$. Midgrid bounceback or midgrid specular reflection boundary conditions are used to impose either hydrodynamic no-slip or free-slip conditions at the other walls, respectively [19]. In order to impose a prescribed velocity or pressure at inlet and outlet boundaries, we impose the equilibrium distribution functions f_i^{eq}, evaluated using the desired hydrodynamic velocity and density values. For our LBM simulations we use unit time step ($\delta t = 1$) and unit grid spacing ($\delta z = \delta r = 1$), hence the length can be measured in terms of the number of nodes. We are using the symmetry boundary condition for the derivative evaluation in Eqs. (13) and (17) at the axis. For the other three boundaries we impose the derivative terms to be zero.

III. NUMERICAL VALIDATION FOR SINGLE-PHASE AXISYMMETRIC LBM

Here we present the validation of the axisymmetric LBM for single-phase flow simulations by comparing it with analytical solutions for the test cases: the axial flow through a tube and the outward radial flow between two parallel discs. These two tests complement each other because they correspond to flows parallel and orthogonal to the axis, respectively. Both flow problems have analytical steady state solutions that help us to validate the accuracy of the axial and radial components of the velocity. All physical quantities in this paper, unless otherwise stated, are reported in lattice units (l.u.), the relaxation time has been keep fixed for all the simulations, $\tau = 1$, and the simulations have been carried out on a rectangular domain of size $H \times R = N_z \times N_r$. The steady state in the following single-phase simulations is defined when the total kinetic energy of the system, $E_{ke} = \pi \sum_{N_z}(\sum_{N_r} r\rho|\mathbf{u}|^2)$, becomes constant up to the machine precision.

A. Flow through a pipe

In this test we consider the constant-density flow of a fluid with density ρ and kinematic viscosity ν flowing inside a circular pipe of radius R. The flow is driven by a constant body force ρg along the the axis of the pipe. The schematic illustration of the flow geometry is presented in Fig. 1. Assuming $u_r(z,r) = 0$ and a no-slip condition on the inner surface ($r = R$) of the pipe, the steady state solution for the axisymmetric NS Eq. (10) for this problem is given by [20]

$$u_z(z,r) = U_1\left[1 - \left(\frac{r}{R}\right)^2\right], \tag{20}$$

where $U_1 = u_r(z,0) = gR^2/(4\nu)$, is the maximum velocity in the pipe.

For the LBM simulation we used the no-slip boundary condition at the inner surface of the pipe, and periodic boundary conditions at the open ends of the pipe. The body force $g = 10^{-5}$ is applied at each node of the simulation domain. The LBM simulations are carried out until the simulation reaches its steady state. The result of the LBM simulation shown in Fig. 2 is in very good agreement with the analytical solution in Eq. (20). This validates the single phase axisymmetric LBM for the case where there is no velocity in the radial direction.

B. Outward radial flow between two parallel discs

Another important test to validate the single-phase axisymmetric LBM is the simulation of the outward radial flow between two parallel discs separated by a distance H. The schematic of the flow setup for this problem is reported in

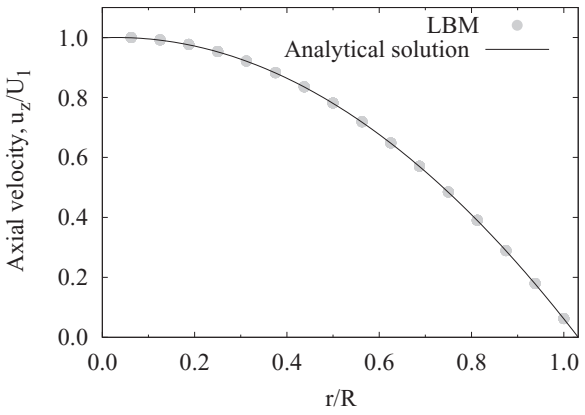

FIG. 2. A comparison of the axial velocity profile as obtained form the LBM simulations (circles) vs the analytical solution (solid line) Eq. (20). Simulation parameters: $N_z \times N_r = 16 \times 16$, $R = N_r$, $\rho = 1$, $\nu = 0.167$, $g = 10^{-5}$, $U_1 = u_z(0) = 3.84 \times 10^{-3}$.

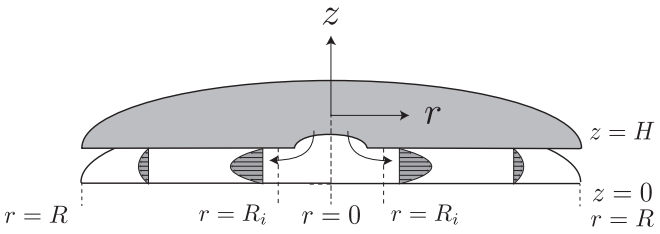

FIG. 3. Schematics of the physical setup to study outward radial flow between two parallel discs. The arrows show the direction of the inlet mass flow. The LBM is used to simulate the flow domain $0 \leqslant z \leqslant H$, $R_i \leqslant r \leqslant R$. We assume that the flow is fully developed for $r \geqslant R_i$ and hence the axial velocity u_z vanishes in this region.

Fig. 3. Assuming $u_z(z,r) = 0$ for $R_i \leqslant r \leqslant R$, the no-slip boundary condition on the discs, and a constant mass flow rate Q along the radial direction, the solution of the NS Eq. (10) corresponding to this problem is given by [20]

$$u_r(z,r) = -U_2 \left(\frac{4R_i}{H^2}\right) \frac{z(z-H)}{r}, \tag{21}$$

where $U_2 = u_r(H/2,R_i) = 3Q/(4\pi R_i H)$. The LBM results shown in Fig. 4 are carried out for the flow domain

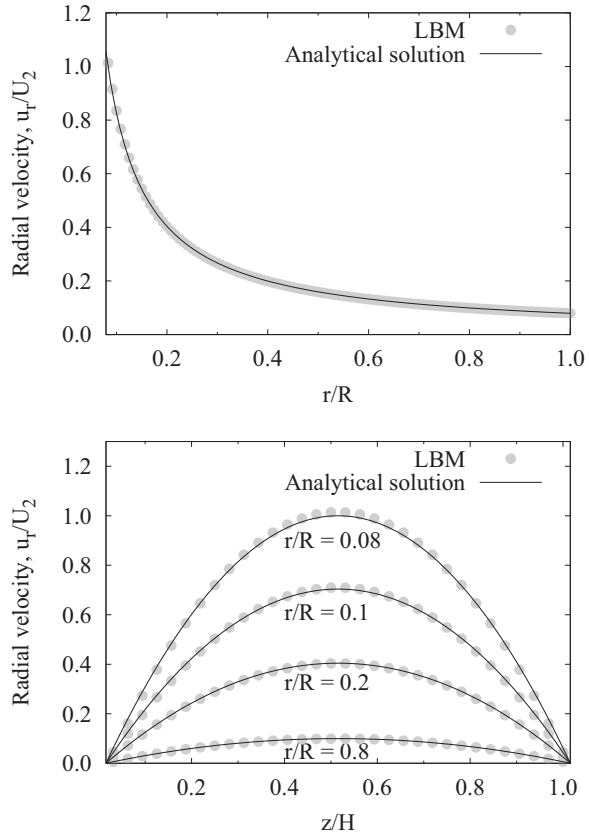

FIG. 4. A comparison of the radial velocity profile u_r as obtained form LBM simulations (circles) vs the analytical solution (solid lines) of Eq. (21). Simulation parameters: $N_z \times N_r = 32 \times 120$, $R = N_r - 0.5$, $H = N_z$, $R_i = 9.5$, $\rho = 1$, $\nu = 0.167$, $Q = 0.5$, and $U_2 = 3.93 \times 10^{-4}$. Top figure shows the comparison at $z = 15.5$. Bottom figure from top to bottom shows the curves correspond to the radial distances $r/R = 0.8$, 0.2, 0.1, and 0.08.

$R_i \leqslant r \leqslant R, 0 \leqslant z \leqslant H$ and using the no-slip boundary condition along the discs. The velocity profile given by Eq. (21) is applied at the inlet boundary while the outlet is considered as an open boundary. The LBM results shown in Fig. 4 are in very good agreement with the analytical solution Eq. (21). This validates the single phase axisymmetric LBM for the case of a radial velocity.

IV. NUMERICAL VALIDATION FOR AXISYMMETRIC MULTIPHASE MODEL

In this section we present the validation for our axisymmetric multiphase LBM for three standard test cases: Laplace law, oscillation of a viscous drop, and the Rayleigh-Plateau (RP) instability.

A. Laplace test

In this validation we compare the in-out pressure differences for different droplet radii. According to the Laplace law the in-out pressure difference Δp for a droplet of radius R_D is given by

$$\Delta p = \frac{2\gamma_{lv}}{R_D}, \tag{22}$$

where γ_{lv} is the liquid-vapor interfacial tension. For this validation we first estimate the value of the surface tension using Eq. (7) (Guo scheme [16]) and Eq. (8) (SC scheme [13]) for both 2D and axisymmetric LBM. The data obtained from these simulations are reported in Table I. Both the Guo and SC scheme are consistent with the fact that for the SC model the surface tension should only depend on the value of the interaction parameter G.

In the next step we do a series of axisymmetric LBM simulations for different droplet radii and measure the in-out pressure difference. When comparing the in-out pressure difference for a drop (Laplace test) and the pressure drop given by Eq. (22), we find that the maximum relative error in pressure difference for the Guo scheme [16] and the SC scheme [13] is 2% and 20%, respectively. This difference might be due to following reason: The external force, $\mathbf{F} \equiv (F_z, F_r)$, can be incorporated in the LBM in several different ways [16,21,22]. However, depending on the chosen forcing scheme, the Chapman-Enskog (CE) expansion has different truncation error terms in the continuity and Navier-Stokes equations. For instance, if one uses the force addition scheme as proposed

TABLE I. Surface tension evaluated using Eq. (8) (columns 2 and 3) and Eq. (7) (columns 4 and 5). Here $\gamma_{lv}^{2D}, \gamma_{lv}^{axis}$ denote the surface tensions obtained from 2D and axisymmetric LBM, respectively. Simulation parameters: $N_z \times N_r = 1 \times 64$, $\tau = 1$, initial interface position, $r = 32$.

G	SC		Guo	
	$\tilde{\gamma}_{lv}^{2D}$	$\tilde{\gamma}_{lv}^{axis}$	γ_{lv}^{2D}	γ_{lv}^{axis}
−4.5	0.0220	0.0220	0.0135	0.0136
−5.0	0.0579	0.0579	0.0376	0.0378
−5.5	0.0995	0.0996	0.0681	0.0683

by Guo *et al.* [16] one obtains the continuity equation given by Eq. (9), whereas by using the scheme proposed by Shan and Chen [12] the CE gives us the following axisymmetric continuity equation:

$$\frac{\partial \rho}{\partial t} + \nabla \cdot (\rho \mathbf{u}) = -\left(\tau - \frac{\delta t}{2}\right) \nabla \cdot \mathbf{F}.$$

Different right hand side terms in the continuity equations result in different densities inside the droplet (in the Laplace test) and one may obtain different pressure, via the equation of state given by Eq. (5). In the axisymmetric continuity equation, with the SC scheme, the gradient operator has an additional term $-(\tau - \frac{\delta t}{2})\frac{F_r}{r}$. Because this term goes as r^{-1} we expect that this may be responsible for the larger numerical errors, thus leading to the departure of about 20% for what concerns the pressure difference.

B. Oscillating droplet

Here we consider the dynamics of the oscillation of an axisymmetric droplet in order to validate the axisymmetric multiphase LBM. We compare the frequency of the oscillation of the droplet obtained from the LBM simulation with the analytical solution reported in Miller and Scriven [23]. The frequency of the second mode for the oscillation of a liquid droplet immersed in another fluid is given by

$$\omega_2 = \omega_2^* - 0.5\alpha(\omega_2^*)^{1/2} + 0.25\alpha^2, \tag{23}$$

where

$$\omega_2^* = \sqrt{\frac{24\gamma_{\rm lv}}{R_{\rm D}^3(2\rho_v + 3\rho_l)}},$$

and $R_{\rm D}$ is the radius of the drop at equilibrium, $\gamma_{\rm lv}$ is the surface tension, ρ_l, ρ_v are the densities of the liquid and vapor phases, respectively. The parameter α is given by

$$\alpha = \frac{25\sqrt{\nu_l \nu_v}\rho_l \rho_v}{\sqrt{2}R_{\rm D}(2\rho_v + 3\rho_l)(\sqrt{\nu_l}\rho_l + \sqrt{\nu_v}\rho_v)},$$

where ν_l, ν_v are the kinematic viscosities of the liquid and vapor phase [23].

In the LBM simulations for this test we use the free-slip boundary condition at the top boundary and periodic boundary conditions at the left and right boundaries. The LBM simulations are initialized with an axisymmetric ellipsoid, $(z/R_a)^2 + (r/R_b)^2 = 1$, where R_a, R_b are the intercepts on the z and r axis, respectively, with total volume $4\pi R_a R_b^2/3$. Due to the surface tension, the ellipsoidal droplet oscillates and due to viscous damping it does finally attain an equilibrium spherical shape with radius $R_{\rm D} = (R_a R_b^2)^{1/3}$ (due to volume conservation). The time evolution of one of these LBM simulations is shown in Fig. 5. The time is measured in the capillary time scale, $t_{\rm cap} = \sqrt{R_{\rm D}^3 \rho_l / \gamma_{\rm lv}}$. The LBM simulations are performed to validate the effect of the droplet size $R_{\rm D}$ on the frequency of oscillation ω_2. In order to calculate the frequency of the oscillation we first measure the length of the intercept on the r axis as a function of time $A(t)$ with $A(t=0) = R_b$, and then we fit the function $g(t) = R_{\rm D} + a\exp(-bt)\sin(\omega_2 t + d)$ (see Fig. 6). We find that the numerical estimation of the frequency of the oscillation of the droplet is in excellent agreement with the theoretically expected value, with a maximum relative error of approximately 1% (see Fig. 6).

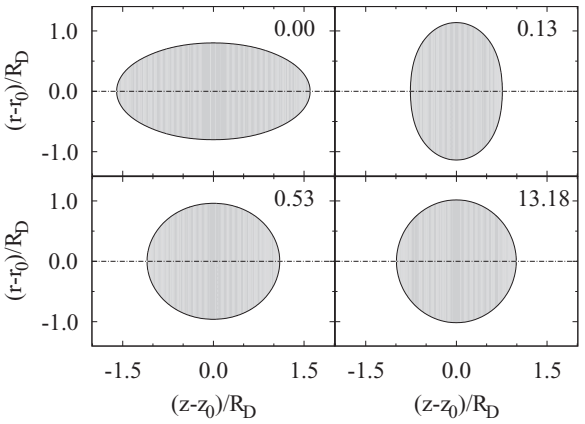

FIG. 5. Time evolution of the shape of an ellipsoidal droplet immersed in a fluid with different density. Simulation parameters: $N_z \times N_r = 320 \times 128$, $G = -6$. $\rho_l = 2.65$, $\rho_v = 0.075$, $(z_0, r_0) = (160.0, 0.5)$. Labels indicate the time corresponding to the different droplet shapes.

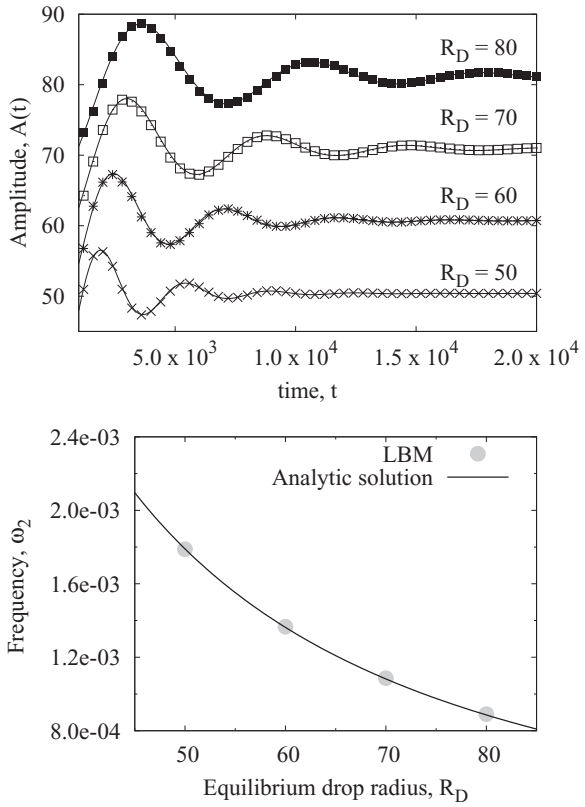

FIG. 6. Top panel: amplitude $A(t)$ of the oscillations vs time t for different equilibrium droplet radii $R_{\rm D}$. Solid lines are obtained by fitting the function $g(t) = R_{\rm D} + a\exp(-bt)\sin(\omega_2 t + d)$ to the data obtained from LBM simulations. Bottom panel: dimensionless frequency of the second mode of oscillation ω_2 vs the equilibrium droplet radius $R_{\rm D}$. Simulation parameters: $N_z \times N_r = 320 \times 128$, $G = -6$.

C. Rayleigh-Plateau (RP) instability

The last problem that we consider for the validation is the breakup of a liquid thread into multiple droplets. The problem was first studied experimentally by Plateau [24] and later theoretically by Lord Rayleigh [25], and is currently referred to as Rayleigh-Plateau (RP) instability. The RP instability has been extensively studied experimentally, theoretically, and numerically [24–27]. Moreover, the problem is fully axisymmetric and therefore suitable for the validation of our multiphase axisymmetric LBM model.

In this validation we check the instability criterion: a liquid cylinder of radius R_C is unstable, if the wavelength of a disturbance λ on the surface of a liquid cylinder is longer then its circumference $2\pi R_C$. Moreover, we compare the radius of the resulting drops with experimental [28] and numerical data [29].

For the LBM simulations we use the free-slip boundary condition at the top boundary and periodic boundary conditions at the left and right boundaries. The LBM simulations are performed in a domain of size $N_z \times N_r = \lambda \times 450$. The wavelength λ of the noise runs over 576, 768, 1024, 1280, 1536, and 1792 for different wave numbers, $\kappa = 2\pi/\lambda$. We represent the wave number in dimensionless form as $\kappa^* = \kappa R_C$. The SC interaction parameter $G = -6.0$, liquid density $\rho_l = 2.68$, vapor density $\rho_v = 0.078$, surface tension $\gamma_{lv} = 0.141$, and kinematic viscosity $\nu = 0.016$ are fixed for these simulations. For these parameters the Ohnesorge number $Oh = \nu\sqrt{\rho_l/(\gamma_{lv} R_C)} = 0.09$. The axial velocity field in the liquid cylinder is initialized by using the sinusoidal velocity field as $u_z(z,r) = \epsilon_u \sin(2\pi z/\lambda)$. For our LBM simulation we use $\epsilon_u < 5 \times 10^{-3}$.

The time evolution of the RP instability corresponding to two different wave numbers $\kappa^* = 2\pi R_C/\lambda$ is shown in Fig. 7. The time is measured in the capillary time scale, $t_{cap} = \sqrt{R_C^3 \rho_l/\gamma_{lv}}$. In our simulations we find that the cylinder breaks up into two or more droplets as long as the condition $\kappa^* < 1$ is satisfied (corresponding to the RP instability criterion, $2\pi R_C < \lambda$). Furthermore, the comparisons of drop sizes for different wave numbers shown in Fig. 8 is in excellent agreement with the results of the slender jet approximation model (SJ) [29] and with experimental data [28].

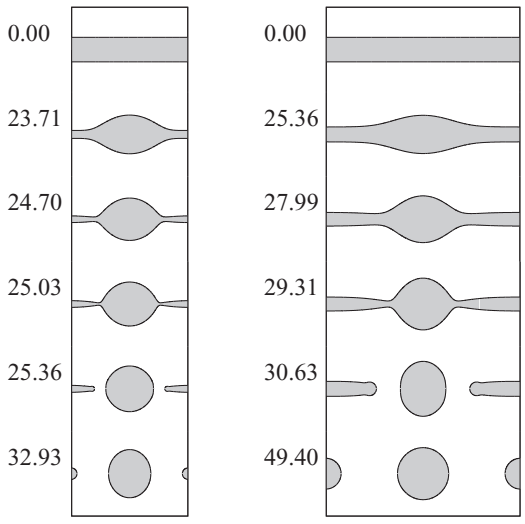

FIG. 7. Growth of the Rayleigh-Plateau instability with time. Left panel: $\kappa^* = 0.65$; right panel: $\kappa^* = 0.39$. Labels on figures indicate the corresponding dimensionless time t/t_{cap}.

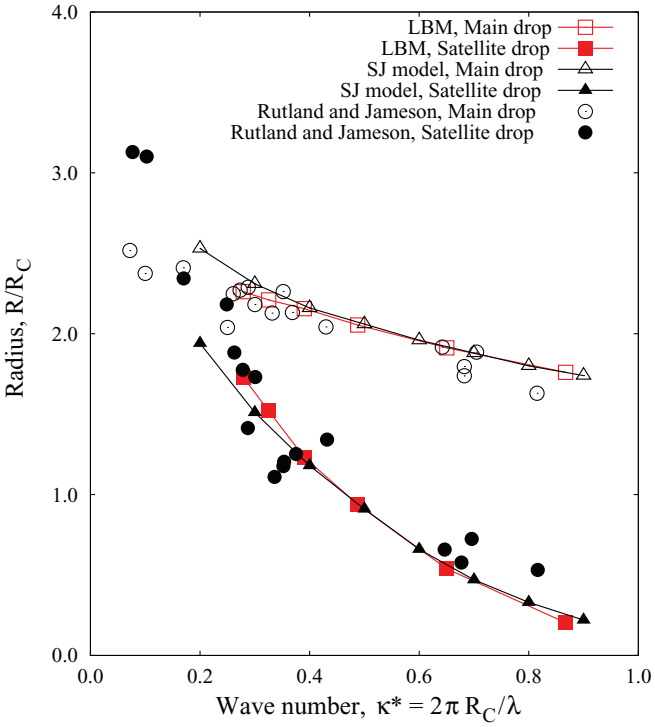

FIG. 8. (Color online) Dimensionless wave number κ^* vs dimensionless droplet radius R/R_C. Triangle markers represents the data obtained from the SJ model for $Oh = 0.1$ [29], circle markers represent the data from experiments [28], and square markers represent data from the axisymmetric LBM simulations for $Oh = 0.09$.

V. CONCLUSIONS

In the present paper we introduced an axisymmetric LBM formulation that can be employed for single-phase as well as for multiphase flows. The multiphase model is the widely employed Shan-Chen model and the axisymmetric version here described is particularly convenient as it allows one to easily switch from 3D to 2D axisymmetric simulations while maintaining the usual Shan-Chen parameters (i.e., densities and coupling strength). The lattice Boltzmann axisymmetric model allows for the solution of multiphase flows at the computational cost of a 2D simulation. One particular interesting application comes from the possibility of increasing the system size, thus reducing the relative size of the LBM diffuse interface with respect to all other length scales in the flow. We presented several validations for single-phase as well as for multiphase flows. In the case of multiphase flows we have quantitatively validated the mass conservation and the dynamics of an axially symmetric oscillating droplet. We have also successfully validated the present model for the contraction of viscous ligament for Re $\sim$ 7 and We $\sim$ 1 [30]. Currently, we are employing the model to study the flow from inkjet nozzles at Re $\sim$ 100 and We $\sim$ 50. Of course there may be limitations on the use of any type of axisymmetric model

concerning higher Re and We number flows. This concerns the case where velocity and/or density may develop fluctuations that break the axisymmetry. These types of flows clearly can never be captured by axisymmetric flows solver. The constraint of axis symmetry may partially be relaxed by models that keep into account azimuthal perturbation to lowest order; this will be the subject of future work.

ACKNOWLEDGMENTS

We acknowledge useful discussions with R. Jeurissen, T. Driessen, and L. Biferale. This work is part of the research program of the Foundation for Fundamental Research on Matter (FOM), which is part of the Netherlands Organization for Scientific Research (NWO).

APPENDIX: CHAPMAN-ENSKOG ON MODIFIED LBM

The modified lattice Boltzmann Eq. (11) for the distribution function $f_i(\mathbf{x},t)$ reads

$$f_i(\mathbf{x}+\mathbf{c}_i\delta t,t+\delta t)-f_i(\mathbf{x},t)=-\frac{1}{\tau}\left[f_i(\mathbf{x},t)-f_i^{\mathrm{eq}}(\rho,\mathbf{u}^{\mathrm{eq}})\right]+\delta t h_i(\mathbf{x}+\mathbf{c}_i\delta t/2,t+\delta t/2), \tag{A1}$$

where h_i is the source terms, $\mathbf{c}_i$ is the lattice velocities, τ is the relaxation parameter, and f_i^{eq} is the discrete second order approximation of the Maxwell-Boltzmann distribution function,

$$f_i^{\mathrm{eq}}(\rho,\mathbf{u})=W_i\rho\left[1+\frac{1}{c_s^2}(\mathbf{c}_i\cdot\mathbf{u})+\frac{1}{2c_s^4}(\mathbf{c}_i\cdot\mathbf{u}^{\mathrm{eq}})^2-\frac{1}{2c_s^2}|\mathbf{u}^{\mathrm{eq}}|^2\right], \tag{A2}$$

where c_s is the speed of sound and W_i's are the weight factors to ensure the symmetry of the lattice. For the D2Q9 LB model with BGK collision operator the speed of sound, $c_s=\sqrt{1/3}$, $W_0=4/9$, $W_i=1/9$ for $i=1,2,3,4$, and $W_i=1/36$ for $i=5,6,7,8$. In general these weights are positive and satisfy following symmetry conditions [31]:

$$\begin{gathered}\sum_i W_i=1,\quad \sum_i W_i c_{i\alpha}=0,\quad \sum_i W_i c_{i\alpha}c_{i\beta}=c_s^2\delta_{\alpha\beta},\quad \sum_i W_i c_{i\alpha}c_{i\beta}c_{i\gamma}=0,\\ \sum_i W_i c_{i\alpha}c_{i\beta}c_{i\gamma}c_{i\delta}=c_s^4(\delta_{\alpha\beta}\delta_{\gamma\delta}+\delta_{\alpha\gamma}\delta_{\beta\delta}+\delta_{\alpha\delta}\delta_{\beta\gamma}),\quad \sum_i W_i c_{i\alpha}c_{i\beta}c_{i\gamma}c_{i\delta}c_{i\eta}=0.\end{gathered} \tag{A3}$$

The hydrodynamic density ρ and momentum ($\rho\mathbf{u}$) are given by the zeroth and first moment of the distribution function respectively, i.e.,

$$\rho(\mathbf{x},t)=\sum_i f_i(\mathbf{x},t), \tag{A4a}$$

$$(\rho\mathbf{u})(\mathbf{x},t)=\sum_i \mathbf{c}_i f_i(\mathbf{x},t). \tag{A4b}$$

In the absence of any external force, $\mathbf{u}^{\mathrm{eq}}=\mathbf{u}$. In order to establish a relation between the LB Eq. (A1) continuity Eq. (9) and the NS equations (10) it is necessary to separate different time scales. We distinguish between slow and fast varying quantities by using two time scales and one space scale [31]. We expand the time and space derivative (∇_c: the gradient operator in the Cartesian coordinate system) using a formal parameter ε as

$$\partial_t=\varepsilon\partial_t^{(1)}+\varepsilon^2\partial_t^{(2)}+O(\varepsilon^3),\quad \nabla_{\mathbf{c}}=\varepsilon\nabla_{\mathbf{c}}^{(1)}+O(\varepsilon^2), \tag{A5}$$

and the distribution function, f_i as

$$f_i=f_i^{(0)}+\varepsilon f_i^{(1)}+\varepsilon^2 f_i^{(2)}+O(\varepsilon^3). \tag{A6}$$

The expansion parameter is formal in the sense that it allows us to keep track of the terms with a different order of magnitude with respect to $f_i^{(0)}$. The zeroth order contribution $f_i^{(0)}$ is exactly the same as the equilibrium distribution function f_i^{eq}. The first and second order perturbations in f_i do not contribute to hydrodynamic density and momentum [31]:

$$\sum_i f_i^{(1)}=\sum_i f_i^{(2)}=0, \tag{A7a}$$

$$\sum_i \mathbf{c}_i f_i^{(1)}=\sum_i \mathbf{c}_i f_i^{(2)}=0. \tag{A7b}$$

The source term h_i does not have any zeroth order contribution and is expanded as

$$h_i=\varepsilon h_i^{(1)}+\varepsilon^2 h_i^{(2)}+O(\varepsilon^3). \tag{A8}$$

Taylor series of f_i and h_i around $(\mathbf{x},t)$ are given by

$$f_i(\mathbf{x}+\mathbf{c}_i\delta t,t+\delta t) = f_i(\mathbf{x},t) + \delta t(\partial_t + c_{i\alpha}\partial_\alpha)f_i(\mathbf{x},t) + \frac{(\delta t)^2}{2}(\partial_t + c_{i\alpha}\partial_\alpha)^2 f_i(\mathbf{x},t) + O[(\delta t)^3], \tag{A9}$$

$$h_i(\mathbf{x}+\mathbf{c}_i\delta t/2,t+\delta t/2) = h_i(\mathbf{x},t) + \frac{\delta t}{2}(\partial_t + c_{i\alpha}\partial_\alpha)h_i(\mathbf{x},t) + \frac{1}{2}\left(\frac{\delta t}{2}\right)^2(\partial_t + c_{i\alpha}\partial_\alpha)^2 h_i(\mathbf{x},t) + O[(\delta t)^3], \tag{A10}$$

where $c_{i\alpha}$ is the αth component of $\mathbf{c}_i$, and ∂_α represents the partial derivative with respect to the αth component of $\mathbf{x}$. Indices $\alpha,\beta,\gamma,\delta$ are used in the following derivation ranges over the set $\{z,r\}$, and when an index appears twice in a single term it represents the standard Einstein summation convention. Using Eqs. (A5), (A6), (A9), and (A10) in Eq. (A1) and rearranging the terms we obtain a series in ε,

$$\begin{aligned}
&\varepsilon\left[\delta t\left(\partial_t^{(1)} f_i^{(0)} + c_{i\alpha}\partial_\alpha^{(1)} f_i^{(0)}\right)\right] + \varepsilon^2\left[\delta t\left(\partial_t^{(2)} f_i^{(0)} + \partial_t^{(1)} f_i^{(1)} + c_{i\alpha}\partial_\alpha^{(1)} f_i^{(1)}\right)\right.\\
&\quad\left. + \frac{(\delta t)^2}{2}\left(\partial_t^{(1)}\partial_t^{(1)} f_i^{(0)} + c_{i\alpha}c_{i\beta}\partial_\alpha^{(1)}\partial_\beta^{(1)} f_i^{(0)} + 2c_{i\alpha}\partial_t^{(1)}\partial_\alpha^{(1)} f_i^{(0)}\right)\right]\\
&= \varepsilon\left[-\frac{1}{\tau}f_i^{(1)} + \delta t h_i^{(1)}\right] + \varepsilon^2\left[-\frac{1}{\tau}f_i^{(2)} + \delta t h_i^{(2)} + \frac{(\delta t)^2}{2}\left(\partial_t^{(1)} + c_{i\alpha}\partial_\alpha^{(1)}\right)h_i^{(1)}\right] + O(\varepsilon^3).
\end{aligned} \tag{A11}$$

Comparing the coefficients of ε, ε^2 and omitting ε^3 terms in Eq. (A11) gives us

$$\delta t\left(\partial_t^{(1)} f_i^{(0)} + c_{i\alpha}\partial_\alpha^{(1)} f_i^{(0)}\right) = -\frac{1}{\tau}f_i^{(1)} + \delta t h_i^{(1)}, \tag{A12}$$

$$\begin{aligned}
&\delta t\left(\partial_t^{(2)} f_i^{(0)} + \partial_t^{(1)} f_i^{(1)} + c_{i\alpha}\partial_\alpha^{(1)} f_i^{(1)}\right) + \frac{(\delta t)^2}{2}\left(\partial_t^{(1)}\partial_t^{(1)} f_i^{(0)} + c_{i\alpha}c_{i\beta}\partial_\alpha^{(1)}\partial_\beta^{(1)} f_i^{(0)} + 2c_{i\alpha}\partial_t^{(1)}\partial_\alpha^{(1)} f_i^{(0)}\right)\\
&= -\frac{1}{\tau}f_i^{(2)} + \delta t h_i^{(2)} + \frac{(\delta t)^2}{2}\left(\partial_t^{(1)} + c_{i\alpha}\partial_\alpha^{(1)}\right)h_i^{(1)},
\end{aligned} \tag{A13}$$

respectively. In the following steps of the CE expansion we will take the zeroth and first lattice velocity moments of Eqs. (A12) and (A13). The zeroth moment of Eqs. (A12) and (A13) will give us the mass conservation up to ε and ε^2 order terms, respectively, and the first moment of Eqs. (A12) and (A13) will give us the momentum conservation up to ε and ε^2 order terms, respectively. Finally by using Eq. (A5) we will obtain equations that conserve the hydrodynamic mass and momentum up to $O(\varepsilon^2)$ perturbations in f_i.

1. Mass conservation

The zeroth order moment is obtained by taking summation of Eq. (A12) over index i, and the first order moment is obtained by multiplying Eq. (A12) by $\mathbf{c}_i$ and taking the summation over index i. The zeroth and first order moments of Eq. (A12) along with Eqs. (A4) and (A7) gives us

$$\partial_t^{(1)}\rho + \partial_\alpha^{(1)}(\rho u_\alpha) = \sum_i h_i^{(1)}, \tag{A14}$$

$$\partial_t^{(1)}(\rho u_\beta) + \partial_\alpha^{(1)}\Pi_{\alpha\beta}^{(0)} = \sum_i c_{i\beta}h_i^{(1)}, \tag{A15}$$

respectively. $\Pi_{\alpha\beta}^{(0)}$ in Eq. (A15) is the zeroth order stress tensor, and using Eq. (A2) it can be expressed in terms of hydrodynamic variables [31]

$$\Pi_{\alpha\beta}^{(0)} \equiv \sum_i c_{i\alpha}c_{i\beta}f_i^{(0)} = \rho\left(c_s^2\delta_{\alpha\beta} + u_\alpha u_\beta\right). \tag{A16}$$

Using Eq. (A16) in Eq. (A15) gives us

$$\partial_t^{(1)}(\rho u_\beta) + \partial_\alpha^{(1)}(\rho u_\alpha u_\beta) = -\partial_\beta\left(c_s^2\rho\right) + \sum_i c_{i\beta}h_i^{(1)}, \tag{A17}$$

Eq. (A14) gives us the density change in convective time scale. In order to estimate the density change in during the diffusive process, we take the zeroth moment of Eq. (A13),

$$\begin{aligned}
&\delta t\left(\partial_t^{(2)}\sum_i f_i^{(0)} + \partial_t^{(1)}\sum_i f_i^{(1)} + \partial_\alpha^{(1)}\sum_i c_{i\alpha}f_i^{(1)}\right) + \frac{(\delta t)^2}{2}\left(\partial_t^{(1)}\partial_t^{(1)}\sum_i f_i^{(0)} + \partial_\alpha^{(1)}\partial_\beta^{(1)}\sum_i c_{i\alpha}c_{i\beta}f_i^{(0)} + 2\partial_t^{(1)}\partial_\alpha^{(1)}\sum_i c_{i\alpha}f_i^{(0)}\right)\\
&= -\frac{1}{\tau}\sum_i f_i^{(2)} + \delta t\sum_i h_i^{(2)} + \frac{(\delta t)^2}{2}\left(\partial_t^{(1)}\sum_i h_i^{(1)} + \partial_\alpha^{(1)}\sum_i c_{i\alpha}h_i^{(1)}\right).
\end{aligned}$$

Using Eqs. (A7), (A4), and (A16) we get

$$\partial_t^{(2)}\rho + \frac{\delta t}{2}\left(\partial_t^{(1)}\partial_t^{(1)}\rho + \partial_\alpha^{(1)}\partial_\beta^{(1)}\Pi_{\alpha\beta}^{(0)} + 2\partial_t^{(1)}\partial_\alpha^{(1)}(\rho u_\alpha)\right) = \sum_i h_i^{(2)} + \frac{\delta t}{2}\left(\partial_t^{(1)}\sum_i h_i^{(1)} + \partial_\alpha^{(1)}\sum_i c_{i\alpha}h_i^{(1)}\right).$$

$$\partial_t^{(2)}\rho + \frac{\delta t}{2}\left[\partial_t^{(1)}\left(\partial_t^{(1)}\rho + \partial_\alpha^{(1)}(\rho u_\alpha)\right) + \partial_\alpha^{(1)}\left(\partial_t^{(1)}(\rho u_\alpha) + \partial_\beta^{(1)}\Pi_{\alpha\beta}^{(0)}\right)\right] = \sum_i h_i^{(2)} + \frac{\delta t}{2}\left(\partial_t^{(1)}\sum_i h_i^{(1)} + \partial_\alpha^{(1)}\sum_i c_{i\alpha}h_i^{(1)}\right).$$

Finally using Eqs. (A14) and (A17) we get

$$\partial_t^{(2)}\rho + \frac{\delta t}{2}\left(\partial_t^{(1)}\sum_i h_i^{(1)} + \partial_\alpha^{(1)}\sum_i c_{i\alpha}h_i^{(1)}\right) = \sum_i h_i^{(2)} + \frac{\delta t}{2}\left(\partial_t^{(1)}\sum_i h_i^{(1)} + \partial_\alpha^{(1)}\sum_i c_{i\alpha}h_i^{(1)}\right). \tag{A18}$$

Rearranging the terms of Eq. (A18) gives us rate of change of density density with diffusive time scale,

$$\partial_t^{(2)}\rho = \sum_i h_i^{(2)}. \tag{A19}$$

We assume that the source term h_i^2 does not change the density at diffusive time scale, i.e.,

$$\sum_i h_i^{(2)} = 0. \tag{A20}$$

Using the relation ε(A14) + ε^2 (A19) we get

$$\partial_t\rho + \partial_\alpha(\rho u_\alpha) = \varepsilon\sum_i h_i^{(1)} + \varepsilon^2\sum_i h_i^{(2)}. \tag{A21}$$

If we choose

$$\varepsilon h_i^{(1)} = -\frac{W_i\rho u_r}{r}, \tag{A22}$$

then

$$\sum_i h_i^{(1)} = -\frac{1}{\varepsilon}\frac{\rho u_r}{r}, \tag{A23a}$$

$$\sum_i c_{i\alpha}h_i^{(1)} = 0, \tag{A23b}$$

$$\sum_i c_{i\alpha}c_{i\beta}h_i^{(1)} = -c_s^2\frac{1}{\varepsilon}\frac{\rho u_r}{r}\delta_{\alpha\beta}. \tag{A23c}$$

Using Eqs. (A21), (A23a), and (A20) gives us

$$\partial_t\rho + \partial_\alpha(\rho u_\alpha) = -\frac{\rho u_r}{r}. \tag{A24}$$

Equation (A24) is the axisymmetric continuity Eq. (9).

2. Momentum conservation

Similarly, in order to calculate the rate of momentum change with respect to diffusive time scale, we take the first moment of Eq. (A13),

$$\begin{aligned}
&\delta t\left(\partial_t^{(2)}\sum_i c_{i\gamma}f_i^{(0)} + \partial_t^{(1)}\sum_i c_{i\gamma}f_i^{(1)} + \partial_\alpha^{(1)}\sum_i c_{i\alpha}c_{i\gamma}f_i^{(1)}\right)\\
&\quad + \frac{(\delta t)^2}{2}\left(\partial_t^{(1)}\partial_t^{(1)}\sum_i c_{i\gamma}f_i^{(0)} + \partial_\alpha^{(1)}\partial_\beta^{(1)}\sum_i c_{i\alpha}c_{i\beta}c_{i\gamma}f_i^{(0)} + 2\partial_t^{(1)}\partial_\alpha^{(1)}\sum_i c_{i\alpha}c_{i\gamma}f_i^{(0)}\right)\\
&= -\frac{1}{\tau}\sum_i c_{i\gamma}f_i^{(2)} + \delta t\sum_i c_{i\gamma}h_i^{(2)} + \frac{(\delta t)^2}{2}\left(\partial_t^{(1)}\sum_i c_{i\gamma}h_i^{(1)} + \frac{\delta t}{2}\partial_\alpha^{(1)}\sum_i c_{i\gamma}c_{i\alpha}h_i^{(1)}\right),
\end{aligned}$$

using Eqs. (A4), (A7), and (A23a) we get

$$\partial_t^{(2)}(\rho u_\gamma)+\partial_\alpha^{(1)}\Pi_{\alpha\gamma}^{(1)}+\frac{\delta t}{2}\left(\partial_t^{(1)}\partial_t^{(1)}(\rho u_\gamma)+\partial_\alpha^{(1)}\partial_\beta^{(1)}P_{\alpha\beta\gamma}^{(0)}+2\partial_t^{(1)}\partial_\alpha^{(1)}\Pi_{\alpha\gamma}^{(0)}\right)=\sum_i c_{i\gamma}h_i^{(2)}-c_s^2\frac{1}{\varepsilon}\partial_\gamma^{(1)}\left(\frac{\rho u_r}{r}\right), \tag{A25}$$

where

$$P_{\alpha\beta\gamma}^{(0)}\equiv\sum_i c_{i\alpha}c_{i\beta}c_{i\gamma}f_i^{(0)}, \tag{A26}$$

$$\Pi_{\alpha\gamma}^{(1)}\equiv\sum_i c_{i\alpha}c_{i\gamma}f_i^{(1)}. \tag{A27}$$

Using Eqs. (A2) and (A3) in Eq. (A26) we get

$$P_{\alpha\beta\gamma}^{(0)}=\frac{1}{c_s^2}\sum_i W_i c_{i\alpha}c_{i\beta}c_{i\gamma}c_{i\delta}(\rho u_\delta)=c_s^2(\delta_{\alpha\beta}(\rho u_\gamma)+\delta_{\beta\gamma}(\rho u_\alpha)+\delta_{\alpha\gamma}(\rho u_\beta)), \tag{A28}$$

and Eq. (A12) in Eq. (A27) gives

$$\Pi_{\alpha\gamma}^{(1)}=\delta t\tau\sum_i c_{i\alpha}c_{i\gamma}\left(h_i^{(1)}-c_{i\delta}\partial_\delta^{(1)}f_i^{(0)}-\partial_t^{(1)}f_i^{(0)}\right)=\delta t\tau\sum_i c_{i\alpha}c_{i\gamma}h_i^{(1)}-\delta t\tau\left(\partial_\delta^{(1)}P_{\alpha\gamma\delta}^{(0)}+\partial_t^{(1)}\Pi_{\alpha\gamma}^{(0)}\right). \tag{A29}$$

Substituting Eqs. (A17) and (A29) in Eq. (A25) and rearranging gives

$$\partial_t^{(2)}(\rho u_\gamma)-\delta t\left(\tau-\frac{1}{2}\right)\left(\partial_\alpha^{(1)}\partial_\delta^{(1)}P_{\alpha\gamma\delta}^{(0)}+\partial_t^{(1)}\partial_\alpha^{(1)}\Pi_{\alpha\gamma}^{(0)}\right)=c_s^2\frac{1}{\varepsilon}\delta t\left(\tau-\frac{1}{2}\right)\partial_\gamma^{(1)}\left(\frac{\rho u_r}{r}\right)+\sum_i c_{i\gamma}h_i^{(2)}. \tag{A30}$$

In order to obtain the NS Eq. (10) from the lattice Boltzmann Eq. (A1) it is necessary that the hydrodynamic velocity satisfies the low Mach number Ma condition, i.e., $O(\mathrm{Ma}^3)$ terms are very small and can be neglected from Eq. (A30). For the LB method the Mach number is defined as $\mathrm{Ma}=u/c_s$, where u is the characteristic hydrodynamic velocity and c_s is the speed of sound in the LB method. The third order velocity appears only in the expression $\partial_t^{(1)}\partial_\alpha^{(1)}\Pi_{\alpha\gamma}^{(0)}$ in Eq. (A30):

$$\begin{aligned}\partial_t^{(1)}\partial_\alpha^{(1)}\Pi_{\alpha\gamma}^{(0)}&=\partial_t^{(1)}\left(\partial_\alpha^{(1)}\Pi_{\alpha\gamma}^{(0)}\right)=\partial_t^{(1)}\left[\partial_\alpha^{(1)}\left(\rho u_\alpha u_\gamma+c_s^2\rho\delta_{\alpha\gamma}\right)\right]=\partial_t^{(1)}\partial_\alpha^{(1)}(\rho u_\alpha u_\gamma)+c_s^2\partial_\gamma^{(1)}\left(\partial_t^{(1)}\rho\right)\\&=\partial_\alpha^{(1)}\left(\partial_t^{(1)}(\rho u_\alpha)u_\gamma+\partial_t^{(1)}(\rho u_\gamma)u_\alpha-\left(\partial_t^{(1)}\rho\right)u_\alpha u_\gamma\right)+c_s^2\partial_\gamma^{(1)}\left(\partial_t^{(1)}\rho\right).\end{aligned}$$

Using Eqs. (A14), (A17), and (A23a) we get

$$\begin{aligned}\partial_t^{(1)}\partial_\alpha^{(1)}\Pi_{\alpha\gamma}^{(0)}&=-\partial_\alpha^{(1)}\left(\left(\partial_t^{(1)}\rho\right)u_\alpha u_\gamma+u_\gamma\partial_\beta^{(1)}\Pi_{\alpha\beta}^{(0)}+u_\alpha\partial_\beta^{(1)}\Pi_{\gamma\beta}^{(0)}\right)-c_s^2\partial_\gamma^{(1)}\left(\partial_\beta^{(1)}(\rho u_\beta)+\frac{1}{\varepsilon}\frac{\rho u_r}{r}\right)\\&=-\partial_\alpha^{(1)}\left[\left(\partial_t^{(1)}\rho\right)u_\alpha u_\gamma+u_\gamma\partial_\beta^{(1)}\left(\rho u_\alpha u_\beta+c_s^2\rho\delta_{\alpha\beta}\right)+u_\alpha\partial_\beta^{(1)}\left(\rho u_\gamma u_\beta+c_s^2\rho\delta_{\gamma\beta}\right)\right]-c_s^2\partial_\gamma^{(1)}\left(\partial_\beta^{(1)}(\rho u_\beta)+\frac{1}{\varepsilon}\frac{\rho u_r}{r}\right)\\&=-\partial_\alpha^{(1)}\left(\left(\partial_t^{(1)}\rho\right)u_\alpha u_\gamma+u_\gamma\partial_\beta^{(1)}(\rho u_\alpha u_\beta)+u_\alpha\partial_\beta^{(1)}(\rho u_\gamma u_\beta)+c_s^2\left(u_\gamma\left(\partial_\alpha^{(1)}\rho\right)+u_\alpha\left(\partial_\gamma^{(1)}\rho\right)\right)\right.\\&\quad\left.-c_s^2\partial_\gamma^{(1)}\left(\partial_\beta^{(1)}(\rho u_\beta)+\frac{1}{\varepsilon}\frac{\rho u_r}{r}\right)\right.\end{aligned}$$

Neglecting the terms $u_\alpha\partial_\beta^{(1)}(\rho u_\beta u_\gamma)$, $(\partial_t^{(1)}\rho)u_\alpha u_\gamma$, and $u_\gamma\partial_\beta^{(1)}(\rho u_\beta u_\alpha)$ (these terms are of order Ma^3) from the last equation we get

$$\partial_t^{(1)}\partial_\alpha^{(1)}\Pi_{\alpha\gamma}^{(0)}=-c_s^2\partial_\alpha^{(1)}\left(u_\gamma\left(\partial_\alpha^{(1)}\rho\right)+u_\alpha\left(\partial_\gamma^{(1)}\rho\right)\right)-c_s^2\partial_\gamma^{(1)}\left(\partial_\beta^{(1)}(\rho u_\beta)+\frac{1}{\varepsilon}\frac{\rho u_r}{r}\right). \tag{A31}$$

Hence using Eqs. (A28) and (A31), the second term on the left hand side of Eq. (A30) becomes

$$\begin{aligned}\partial_\alpha^{(1)}\partial_\delta^{(1)}P_{\alpha\gamma\delta}^{(0)}+\partial_t^{(1)}\partial_\alpha^{(1)}\Pi_{\alpha\gamma}^{(0)}&=c_s^2\left(\partial_\delta^{(1)}\partial_\delta^{(1)}\left(\rho u_\gamma\right)+2\partial_\delta^{(1)}\partial_\gamma^{(1)}(\rho u_\delta)\right)-c_s^2\partial_\alpha^{(1)}\left(u_\gamma\left(\partial_\alpha^{(1)}\rho\right)\right.\\&\quad\left.+u_\alpha\left(\partial_\gamma^{(1)}\rho\right)+\partial_\gamma^{(1)}(\rho u_\beta)\right)-c_s^2\frac{1}{\varepsilon}\partial_\gamma^{(1)}\left(\frac{\rho u_r}{r}\right);\end{aligned}$$

rearranging the terms we get

$$\begin{aligned}
&\partial_\alpha^{(1)}\partial_\delta^{(1)}P^{(0)}_{\alpha\gamma\delta}+\partial_t^{(1)}\partial_\alpha^{(1)}\Pi^{(0)}_{\alpha\gamma}\\
&=c_s^2\big(\partial_\delta^{(1)}\partial_\delta^{(1)}(\rho u_\gamma)+2\partial_\delta^{(1)}\partial_\gamma^{(1)}(\rho u_\delta)-\partial_\beta^{(1)}\big(u_\gamma\partial_\alpha^{(1)}\rho\big)-\partial_\beta^{(1)}\big(u_\alpha\partial_\gamma^{(1)}\rho\big)-\partial_\beta^{(1)}\partial_\gamma^{(1)}(\rho u_\beta)\big)-c_s^2\frac{1}{\varepsilon}\partial_\gamma^{(1)}\left(\frac{\rho u_r}{r}\right)\\
&=c_s^2\big(\partial_\delta^{(1)}\partial_\delta^{(1)}(\rho u_\gamma)+\partial_\delta^{(1)}\partial_\gamma^{(1)}(\rho u_\delta)-\partial_\beta^{(1)}\big(u_\gamma\partial_\alpha^{(1)}\rho\big)-\partial_\beta^{(1)}\big(u_\alpha\partial_\gamma^{(1)}\rho\big)\big)-c_s^2\frac{1}{\varepsilon}\partial_\gamma^{(1)}\left(\frac{\rho u_r}{r}\right)\\
&=c_s^2\big(\partial_\delta^{(1)}\big(\rho\partial_\delta^{(1)}u_\gamma\big)+\partial_\delta^{(1)}\big(\rho\partial_\gamma^{(1)}u_\delta\big)\big)-c_s^2\frac{1}{\varepsilon}\partial_\gamma^{(1)}\left(\frac{\rho u_r}{r}\right).
\end{aligned}\tag{A32}$$

Substituting Eq. (A32) back in to Eq. (A30) gives us

$$\begin{aligned}
&\partial_t^{(2)}(\rho u_\gamma)-c_s^2\delta t\left(\tau-\frac{1}{2}\right)\big(\partial_\delta^{(1)}\big(\rho\partial_\delta^{(1)}u_\gamma\big)+\partial_\delta^{(1)}\big(\rho\partial_\gamma^{(1)}u_\delta\big)\big)+c_s^2\frac{1}{\varepsilon}\delta t\left(\tau-\frac{1}{2}\right)\partial_\gamma^{(1)}\left(\frac{\rho u_r}{r}\right)\\
&\quad=c_s^2\frac{1}{\varepsilon}\delta t\left(\tau-\frac{1}{2}\right)\partial_\gamma^{(1)}\left(\frac{\rho u_r}{r}\right)+\sum_i c_{i\gamma}h_i^{(2)}.
\end{aligned}\tag{A33}$$

Using Eq. (A23a) and rearranging we get

$$\partial_t^{(2)}(\rho u_\gamma)=c_s^2\delta t\left(\tau-\frac{1}{2}\right)\partial_\delta^{(1)}\big[\rho\big(\partial_\delta^{(1)}u_\gamma+\partial_\gamma^{(1)}u_\delta\big)\big]+\sum_i c_{i\gamma}h_i^{(2)}.\tag{A34}$$

Using the relation ε (A17) + ε^2 (A34) along with Eq. (A5) we get

$$\partial_t(\rho u_\gamma)+\partial_\alpha(\rho u_\alpha u_\gamma)=-\partial_\gamma\big(c_s^2\rho\big)+c_s^2\delta t\left(\tau-\frac{1}{2}\right)\partial_\delta\big[\rho\big(\partial_\delta u_\gamma+\partial_\gamma u_\delta\big)\big]+\varepsilon^2\sum_i c_{i\gamma}h_i^{(2)}.\tag{A35}$$

If we define $\nu=c_s^2\delta t(\tau-0.5)$ and $p=c_s^2\rho$ Eq. (A35) becomes

$$\partial_t(\rho u_\gamma)+\partial_\alpha(\rho u_\alpha u_\gamma)=-\partial_\gamma p+\nu\partial_\delta[\rho(\partial_\delta u_\gamma+\partial_\gamma u_\delta)]+\varepsilon^2\sum_i c_{i\gamma}h_i^{(2)}.\tag{A36}$$

Equation (A36) represents the axisymmetric NS equation if the source term $h_i^{(2)}$ satisfies the following conditions:

$$\varepsilon^2\sum_i c_{ir}h_i^{(2)}=2\mu\partial_r\left(\frac{u_r}{r}\right)-\frac{\rho u_r^2}{r},\tag{A37}$$

$$\varepsilon^2\sum_i c_{iz}h_i^{(2)}=\frac{\mu}{r}(\partial_r u_z+\partial_z u_r)-\frac{\rho u_r u_z}{r}.\tag{A38}$$

Finally we summarize the conditions on $h_i^{(1)}$ and $h_i^{(2)}$ that give us the axisymmetric NS equation in the long-wavelength and small Mach number limit:

$$\sum_i h_i^{(1)}=-\frac{1}{\varepsilon}\frac{\rho u_r}{r},\quad \sum_i c_{ir}h_i^{(1)}=0,\quad \sum_i c_{iz}h_i^{(1)}=0,$$

and

$$\sum_i h_i^{(2)}=0,\quad \sum_i c_{ir}h_i^{(2)}=\frac{1}{\varepsilon^2}\left[2\mu\partial_r\left(\frac{u_r}{r}\right)-\frac{\rho u_r^2}{r}\right],\quad \sum_i c_{iz}h_i^{(2)}=\frac{1}{\varepsilon^2}\left(\frac{\mu}{r}(\partial_r u_z+\partial_z u_r)-\frac{\rho u_r u_z}{r}\right),$$

hence

$$\begin{aligned}
h_i&=\varepsilon h_i^{(1)}+\varepsilon^2 h_i^{(2)},\\
&=W_i\left(-\frac{\rho u_r}{r}+\frac{1}{c_s^2}\big(c_{iz}H_z+c_{ir}H_r\big)\right),
\end{aligned}$$

which is the same as Eq. (13). This ends our Chapman-Enskog expansion procedure to obtain the axisymmetric NS from the modified LB equation. We do not impose any additional condition on the density of fluid ρ.

[1] H. Wijshoff, Phys. Rep. **491**, 77 (2010).

[2] S. Succi, *The Lattice Boltzmann Equation for Fluid Dynamics and Beyond* (Oxford University Press, New York, 2001).

[3] S. Chen and G. D. Doolen, Annu. Rev. Fluid Mech. **30**, 329 (1998).

[4] I. Halliday, L. A. Hammond, C. M. Care, K. Good, and A. Stevens, Phys. Rev. E **64**, 011208 (2001).

[5] T. Reis and T. N. Phillips, Phys. Rev. E **75**, 056703 (2007).
[6] H. Huang and X.-Y. Lu, Phys. Rev. E **80**, 016701 (2009).
[7] Z. Guo, H. Han, B. Shi, and C. Zheng, Phys. Rev. E **79**, 046708 (2009).
[8] Q. Li, Y. L. He, G. H. Tang, and W. Q. Tao, Phys. Rev. E **81**, 056707 (2010).
[9] S. Chen, J. Tölke, S. Geller, and M. Krafczyk, Phys. Rev. E **78**, 046703 (2008).
[10] K. N. Premnath and J. Abraham, Phys. Rev. E **71**, 056706 (2005).
[11] S. Mukherjee and J. Abraham, Phys. Rev. E **75**, 026701 (2007).
[12] X. Shan and H. Chen, Phys. Rev. E **47**, 1815 (1993).
[13] X. Shan and H. Chen, Phys. Rev. E **49**, 2941 (1994).
[14] X. He and G. Doolen, J. Stat. Phys. **107**, 309 (2002).
[15] R. Benzi, L. Biferale, M. Sbragaglia, S. Succi, and F. Toschi, Phys. Rev. E **74**, 021509 (2006).
[16] Z. Guo, C. Zheng, and B. Shi, Phys. Rev. E **65**, 046308 (2002).
[17] T. Reis and T. N. Phillips, Phys. Rev. E **76**, 059902(E) (2007).
[18] T. Reis and T. N. Phillips, Phys. Rev. E **77**, 026703 (2008).
[19] M. Sukop and D. Thorne, *Lattice Boltzmann Modeling: An Introduction for Geoscientists and Engineers* (Springer-Verlag, Berlin, 2006).
[20] S. Middleman, *Modeling Axisymmetric Flows: Dynamics of Films, Jets, and Drops* (Academic, New York, 1995).
[21] J. M. Buick and C. A. Greated, Phys. Rev. E **61**, 5307 (2000).
[22] H. Huang, M. Krafczyk, and X. Lu, Phys. Rev. E **84**, 046710 (2011).
[23] C. Miller and L. Scriven, J. Fluid Mech. **32**, 417 (1968).
[24] J. Plateau, in *Statique Expérimentale et Théoretique des Liquides Soumis aux Seules Forces Moléculaires*, Vol. II (Gauthier Villars, Paris, 1873), p. 319.
[25] J. W. S. Lord Rayleigh, Proc. Lond. Math. Soc. **10**, 4 (1879).
[26] P. Lafrance, Phys. Fluids **18**, 428 (1975).
[27] S. Tomotika, Proc. R. Soc. London A **150**, 322 (1935).
[28] D. F. Rutland and G. J. Jameson, J. Fluid Mech. **46**, 267 (2006).
[29] T. Driessen and R. Jeurissen, Int. J. Comp. Fluid Dyn. **25**, 333 (2011).
[30] S. Srivastava, T. Driessen, R. Jeurissen, H. Wijshoff, and F. Toschi, arXiv:1305.6189.
[31] D. A. Wolf-Gladrow, *Lattice Gas Cellular Automata and Lattice Boltzmann Models*, Vol. 1725 of Lecture Notes in Mathematics (Springer-Verlag, Berlin, 2000).